

Oxidation State of Single-Atom Re/TiO₂ Hydrogenation Catalysts A Computational Study

Sreenithya, A.; Kolganov, Alexander A.; Yeu, In Won; Risansyauqi, Muhammad Helmi; Pidko, Evgeny A.

DOI

[10.1021/acscatal.4c05697](https://doi.org/10.1021/acscatal.4c05697)

Publication date

2024

Document Version

Final published version

Published in

ACS Catalysis

Citation (APA)

Sreenithya, A., Kolganov, A. A., Yeu, I. W., Risansyauqi, M. H., & Pidko, E. A. (2024). Oxidation State of Single-Atom Re/TiO₂ Hydrogenation Catalysts: A Computational Study. *ACS Catalysis*, 14(24), 18488-18498. <https://doi.org/10.1021/acscatal.4c05697>

Important note

To cite this publication, please use the final published version (if applicable).
Please check the document version above.

Copyright

Other than for strictly personal use, it is not permitted to download, forward or distribute the text or part of it, without the consent of the author(s) and/or copyright holder(s), unless the work is under an open content license such as Creative Commons.

Takedown policy

Please contact us and provide details if you believe this document breaches copyrights.
We will remove access to the work immediately and investigate your claim.

Oxidation State of Single-Atom Re/TiO₂ Hydrogenation Catalysts: A Computational Study

A. Sreenithya,* Alexander A. Kolganov, In Won Yeu, Muhammad Helmi Risansyaqi, and Evgeny A. Pidko*



Cite This: *ACS Catal.* 2024, 14, 18488–18498



Read Online

ACCESS |

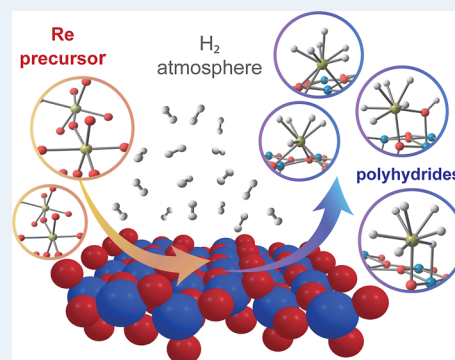
Metrics & More

Article Recommendations

Supporting Information

ABSTRACT: Supported rhenium (Re) catalysts are emerging as promising candidates for hydrogenation reactions, which are crucial in industrial processes such as biomass valorization, CO₂ reduction, and petroleum refining. However, despite their broad application, the structural and mechanistic understanding of these systems remains limited. The strong oxophilic nature of Re, combined with its ability to adopt multiple oxidation states, complicates the characterization of the active species even with advanced experimental techniques. In this study, we employ density functional theory calculations, alongside *ab initio* thermodynamic analysis, to systematically explore the structural and electronic properties of single-atom Re catalysts on a TiO₂ surface, providing insights that could inform the rational catalyst design. Our calculations reveal the formation of stable Re polyhydrides on the surface under hydrogen-rich conditions. Notably, even in highly reducing environments, Re species with low formal oxidation states are thermodynamically unfavorable. The stable Re species identified on TiO₂ surfaces demonstrate high reactivity toward CO₂ hydrogenation. The electronic properties and computed X-ray photoelectron spectroscopy (XPS) signatures of the feasible surface species are highly influenced by the ligand environment. This work highlights the limitation of routine interpretation of experimental XPS characterization data in terms of the formal oxidation state.

KEYWORDS: hydrogenation reaction, supported rhenium catalysis, TiO₂ surface, heterogeneous catalysis, density functional theory, *ab initio* thermodynamic model



1. INTRODUCTION

Supported rhenium (Re) catalysts exhibit remarkable activity and selectivity in hydrogenation reactions, making them promising candidates for contemporary industrial processes to produce value-added chemicals.^{1,2} They are extensively utilized in the valorization of biomass-derived molecules through hydrogenolysis and deoxygenation reactions (Figure 1).³ Rhenium catalysts facilitate hydrodesulfurization and hydrodenitrogenation, crucial processes for reducing sulfur and nitrogen impurities in the petroleum feedstock.^{4–6} Another noteworthy application of supported rhenium catalysts is in cross-alkane metathesis, a key step in polyethylene recycling processes.^{7,8} Recently, titanium dioxide-supported Re (Re/TiO₂) catalysts have been reported to outperform the industrially employed Cu/ZnO/Al₂O₃ catalysts for CO₂ reduction at low reaction temperature (below 200 °C).^{9,10} Despite these wide-ranging applications, crucial structural and mechanistic insights, particularly regarding the nature of the active sites, remain limited in these catalytic systems. Detailed investigations of Re catalysts focusing on these aspects could significantly advance and optimize their use through rational catalyst design.

Determining the exact nature of the Re species formed on a support is challenging. Despite the application of sophisticated analytical methods, the structures, oxidation states, and geometries of these species remain unclear. Depending on reaction conditions, the active species formed on a surface can vary in the number of Re atoms and their oxidation states as well as their specific local environment. Most of the advanced characterization studies point to the important role of atomically dispersed Re on the support.¹¹ For example, in Re-catalyzed olefin metathesis using oxide supports such as SiO₂ and Al₂O₃, the active species are predominantly single-atom Re species.^{12–14} Recent research has shown that the selectivity in CO₂ reduction is highly sensitive to Re catalyst loading on TiO₂ and In₂O₃.^{9,15} Characterization of these systems revealed highly dispersed Re, with a proposed methanol selectivity originating from isolated Re active sites.

Received: September 17, 2024

Revised: November 19, 2024

Accepted: November 26, 2024

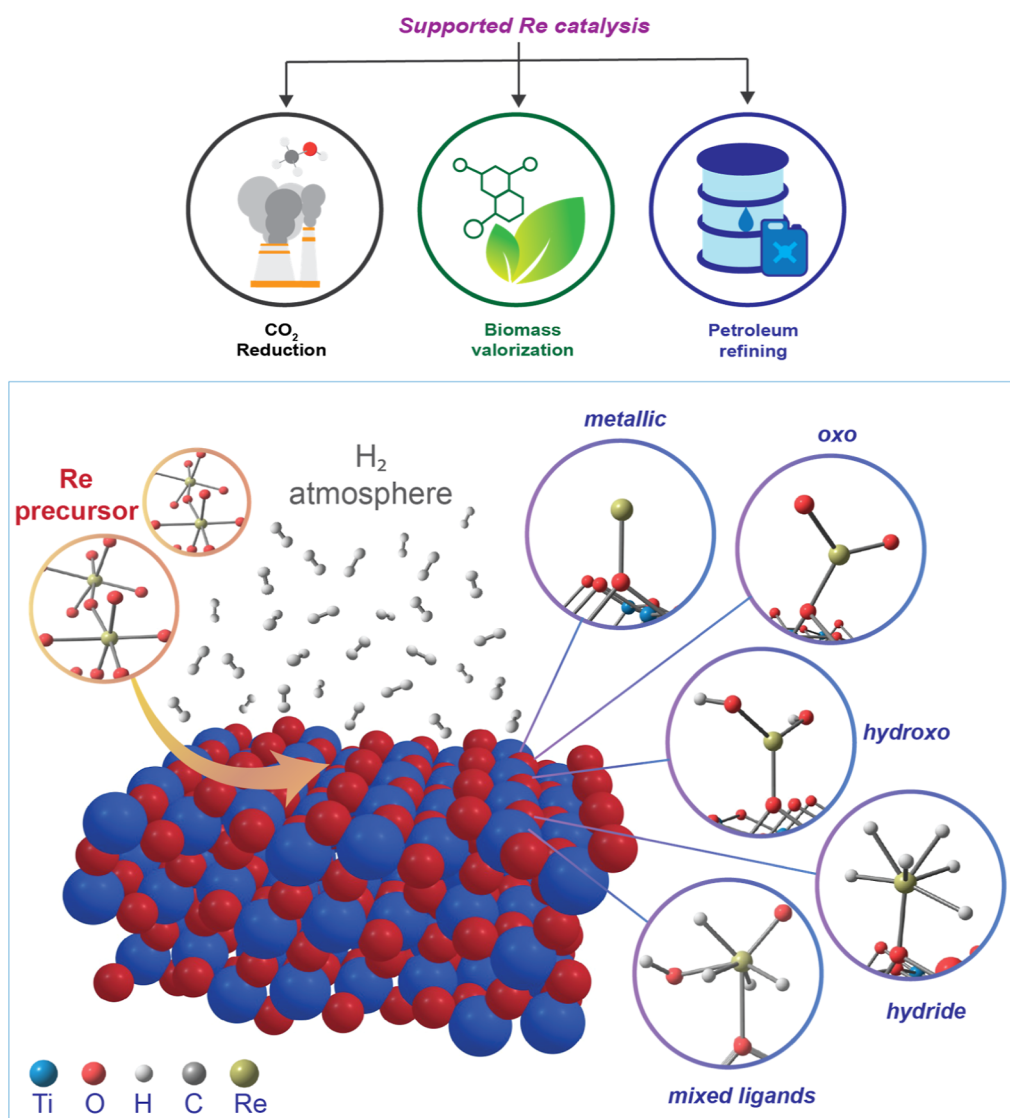


Figure 1. Supported rhenium-catalyzed hydrogenation has a wide range of applications, including CO₂ reduction, biomass valorization, and petroleum refining. When introduced onto the TiO₂ surface, the rhenium precursor can form various active sites. These include species with different ligands at the metal center and varying oxidation states, such as metallic rhenium, oxo, hydroxo, hydride, and mixed ligand-coordinated species.

Similar atomically dispersed Re species were detected in bimetallic catalytic systems for the hydrogenation of vicinal diols, carboxylic acids, and esters.^{16–18}

The highly oxophilic nature and multiple possible oxidation states of Re, ranging from -3 to $+7$, enable flexible catalytic speciation and unique reactivity. However, this diverse range of oxidation states complicates the characterization of Re catalysts, limiting a comprehensive understanding of these species. Previous studies often proposed metallic Re⁰ species as the active sites for H₂ activation and hydrogenation processes. However, most spectral analyses suggest oxidized Re species over metallic Re. These analyses also indicate the coexistence of multiple oxidation states, further complicating the understanding.^{19–22} For instance, in the deoxygenation of vicinal diols to alkene, Re⁴⁺ and Re⁶⁺ species were detected on a CeO₂ support via X-ray photoelectron spectroscopy (XPS).²³ Multiple oxidized Re species, including Re²⁺, Re⁴⁺, Re⁵⁺, and Re⁶⁺, were identified in bimetallic catalysis for ester hydrogenation.^{17,24} An XPS study of a Re/TiO₂ catalyst for CO₂

hydrogenation showed Re⁰, Re^{δ+}–Re¹⁺, Re²⁺, Re⁴⁺, and Re⁶⁺ species,¹⁰ while another study proposed the existence of Re⁷⁺ species along with Re⁴⁺ and Re⁶⁺.²⁵ These reports highlight that despite extensive efforts, significant ambiguities remain regarding the nature of the Re catalytic active species.

Re-based hydrogenation catalysts are synthesized mostly by impregnation of the support by Re precursors such as Re₂O₇ and NH₄ReO₄. The resulting Re/TiO₂ catalyst is prereduced under a H₂ atmosphere before employing it for the hydrogenation reaction. This could lead to the formation of a multitude of possible chemical combinations for active species with varying ligands and Re oxidation states. This could involve the reduction of oxygen ligands on Re to hydroxo, replacement of hydroxo ligands with a hydride or reduction of the metal center by eliminating water etc., under a H₂ atmosphere (Figure 1). A detailed analysis of these systems may lead to a better understanding of Re speciation under relevant reaction conditions of hydrogenation reactions. In this study, we employ density functional theory (DFT) calculations

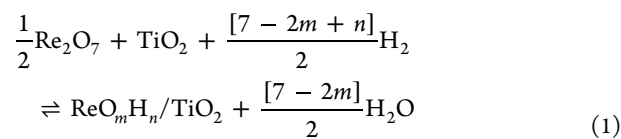
complimented by ab initio thermodynamic analysis (aiTD) for the systematic analysis of feasible Re active species formed on TiO₂, one of the widely employed catalyst supports in hydrogenation reactions. Specifically, we are interested in the effect of different coordination environments on the electronic structure of Re active sites.

2. COMPUTATIONAL METHODS

2.1. DFT Methods. All spin-polarized DFT calculations were performed using the Vienna Ab initio Simulation Package (VASP 5.4.4).^{26,27} The electron exchange–correlation was represented by the generalized gradient approximation with the Perdew–Burke–Ernzerhof (PBE) exchange–correlation functional. The projected augmented wave method was employed to model the ion–electron interactions for all atoms. For Re, a GW potential was employed to achieve a better geometry convergence. The DFT + *U* method was applied to the 3d orbitals of Ti to correct the self-interaction error in DFT, using a Hubbard *U* value of 3.5 eV as recommended in the literature.²⁸ A plane wave basis set with a kinetic energy cutoff of 400 eV was used for all of the calculations. The Brillouin zone sample was reduced to the Γ point. The convergence energy threshold for each iteration was set to 10^{−5} eV. Geometries were considered converged when the forces on each atom were less than 0.05 eV Å^{−1}. During the iterative diagonalization of the Kohn–Sham Hamiltonian, Gaussian smearing with a width of 0.10 eV was applied for the population of partial occupancies.

2.2. Models. The bulk TiO₂ unit cell in the phase of anatase was fully optimized initially. The anatase form of TiO₂ is known to perform as a better catalyst support due to its higher surface area and better catalyst–support interaction and stability.²⁹ The optimized lattice vectors of *a* = 3.799, *b* = 3.799, and *c* = 9.716 with $\alpha = \beta = \gamma = 90^\circ$ have a good agreement with the experiment parameters.³⁰ A 2 × 4 supercell of the anatase TiO₂(101) surface with a vacuum space of 15 Å was employed in this study. The anatase TiO₂(101) surface has higher stability compared to other surfaces and is known to promote many chemical conversions.^{31–36} These slab models contained six titanium layers, with the bottom three layers fixed while the remaining layers were allowed to relax during geometry optimization.³⁷ A perfect (TiO₂-p) as well as defect-containing partially reduced titania (TiO₂-d) surfaces were employed in the calculations to understand the role of defects. A defective TiO₂-d surface was created by forming an oxygen vacancy, achieved by removing a 2-fold coordinated oxygen (O_{2c}) atom that connects a 5-fold and 6-fold coordinated Ti (Ti_{5c} and Ti_{6c}, respectively) atom on the surface (Figure 3a). All geometries were built manually by systematically varying the ligands around Re for different formal oxidation states (0 to +7), and for each structure, neutral charge was assigned.

2.3. aiTD Analysis. aiTD analysis was performed to account for the temperature and pressure effects on the stability of different surface-active species in the presence of hydrogen and water. Bulk Re₂O₇ and a bare TiO₂-p/TiO₂-d support were used as the reference species in this analysis. Water is produced during the formation of active species by the reduction of oxygen ligands on the Re. The equilibria established between the reference Re₂O₇ and different surface-active species could be formulated by a general form as shown in eq 1.



The reaction Gibbs free energy at temperature *T* and pressure *P* for the equilibrium $\Delta G(T, p)$ is calculated as

$$\Delta G(T, p) = G_{\text{ReO}_m\text{H}_n/\text{TiO}_2}^{\text{S}} - \frac{1}{2}G_{\text{Re}_2\text{O}_7}^{\text{S}} - G_{\text{TiO}_2}^{\text{S}} - [7 - 2m + n]\mu_{\text{H}}^{\text{g}} + \frac{[7 - 2m]}{2}\mu_{\text{H}_2\text{O}}^{\text{g}} \quad (2)$$

The superscripts S and g in eq 2 stand for the solid and gas phase, respectively. In this model, the vibrational and pressure–volume contributions of solids were neglected, and their Gibbs free energies were approximated as the corresponding DFT computed electronic energies. The potential impact of zero-point energy (ZPE) contributions known for hydroxyl ligands was analyzed in selected Re species. While the inclusion of ZPE corrections affected the energy gaps between species, the overall energy trends remained consistent (Figure S6 in the Supporting Information). The chemical potential of hydrogen and water in the gas phase depends on *T* and *P*. The H₂ atmosphere is assumed to be an ideal-gas-like reservoir and choose the reference state of $\Delta\mu_{\text{H}}(T, P)$ to be the total electronic energy of an isolated H₂ molecule, i.e., the chemical potential of hydrogen at the reference state of 0 K, $\Delta\mu_{\text{H}}(0 \text{ K}) = \frac{1}{2}E_{\text{H}_2}$, where *E*_{H₂} is the DFT calculated total electronic energy of H₂. Then, the chemical potential of hydrogen at *T* and *P* is

$$\mu_{\text{H}}^{\text{g}}(T, P) = \frac{1}{2}E_{\text{H}_2} + \Delta\mu_{\text{H}}^{\text{g}}(T, P) \quad (3)$$

where

$$\begin{aligned} \Delta\mu_{\text{H}}^{\text{g}}(T, P) &= \Delta\mu_{\text{H}}(T, P^0) + \frac{1}{2}RT \ln \left(\frac{P_{\text{H}_2}}{P_{\text{H}_2}^0} \right) \\ &= \frac{1}{2} \left[\Delta\mu_{\text{H}_2}(T, P^0) + RT \ln \left(\frac{P_{\text{H}_2}}{P_{\text{H}_2}^0} \right) \right] \\ &= \frac{1}{2} \left[[H(T, P^0, \text{H}_2) - H(0 \text{ K}, P^0, \text{H}_2)] \right. \\ &\quad \left. - T(S(T, P^0, \text{H}_2) - S(0 \text{ K}, P^0, \text{H}_2)) \right. \\ &\quad \left. + RT \ln \left(\frac{P_{\text{H}_2}}{P_{\text{H}_2}^0} \right) \right] \quad (4) \end{aligned}$$

The temperature and pressure dependency of the chemical potential is gained from the differences in the enthalpy (*H*) and entropy (*S*) with respect to the reference state at 0 K. For a standard pressure of 1 bar, the entropy and enthalpy values tabulated in the thermodynamic tables were employed.³⁸

Similarly, the chemical potential of water is calculated as

$$\mu_{\text{H}_2\text{O}}^{\text{g}}(T, P) = E_{\text{H}_2\text{O}} + \Delta\mu_{\text{H}_2\text{O}}^{\text{g}}(T, P) \quad (5)$$

Bringing 3 and 5 to 2, the reaction Gibbs free energy is

The geometries of various Re active species on the support were computed by using periodic DFT methods. Detailed reaction pathways for the formation of each species are provided in Scheme S1 in the [Supporting Information](#). On the surface, Re species can adopt two distinct geometries: mono- and bidentate binding with the surface oxygen atoms. In the monodentate configuration, the Re center is coordinated to a single 2-fold coordinated oxygen atom (O_{2c}), whereas in the bidentate structure, Re is bound to two such oxygen atoms, as depicted in [Figure 3b](#). Calculations indicate that the bidentate

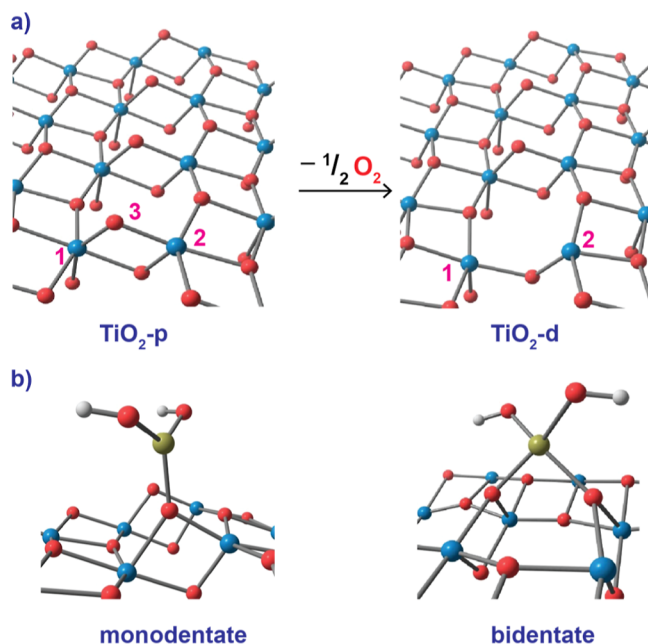


Figure 3. (a) Removal of a 2-fold oxygen 3 coordinated to titanium 1 and 2 on a perfect titania surface (TiO_2 -p) results in a defective (TiO_2 -d) surface with an oxygen vacancy. 6-fold (1) and 5-fold (2) coordinated Ti^{4+} on TiO_2 -p reduce to 5-fold and 4-fold Ti^{3+} on TiO_2 -d; (b) representative surface active species $Re(OH)_2$ in monodentate and bidentate configuration.

geometry is energetically favored, with a stability advantage of 0.08 to 0.68 eV over the monodentate configuration. However, as the coordination environment around the Re center becomes more crowded, either due to the increased number of ligands or the presence of sterically demanding, electron-rich oxygen ligands, the monodentate configuration becomes energetically preferable. For instance, while all hydrides (ReH_y) with $y = 1$ to 6 favor a bidentate geometry, ReH_7 prefers a monodentate configuration. In the case of $Re(IV)$ species, most adopt a bidentate geometry, with the exception of ReO_2 , which shifts to a monodentate geometry. Similarly, among $Re(V)$ species, ReH_5 favors a bidentate configuration, while $Re(OH)H_4$, $Re(OH)_2H_3$, and $ReO(OH)H_2$ exhibit comparable energies for both mono- and bidentate forms. Conversely, $ReO_2(OH)$ adopts a monodentate configuration. See Tables S1 and S2 and Figures S1 and S2 in the [Supporting Information](#) for the calculated formation energies for various Re active species, details on conformational analysis, and energetic comparison between mono- and bidentate geometries.

3.2. aiTD Analysis. To provide insight into the nature of active species formed under relevant reaction conditions, we employed aiTD analysis on the DFT calculated species. The

lowest-energy conformer of each active species formed under reducing conditions as shown in [eq 1](#) was used to construct the aiTD model. Under these conditions, the oxygen ligands on Re are hydrogenated to form hydroxide, exchanged to form hydrides, or eliminated as water. Stability of the resulting surface species is analyzed using the aiTD model.

The results of aiTD analysis for TiO_2 -d model supports are summarized in [Figure 4](#). As the precatalyst is reduced with hydrogen, active species formation is analyzed with respect to the change in the chemical potential of hydrogen ($\Delta\mu_H$). Under oxidizing conditions resembling the unactivated as-prepared precatalyst, Re is stabilized on both TiO_2 -p and TiO_2 -d supports in the oxygenated ReO_3 state. Independent of the support model TiO_2 -d or TiO_2 -p, our analysis identifies polyhydride Re species with a formal oxidation state +5 to +7 as the most stable species in a H_2 -rich environment. On a defected TiO_2 surface, Re polyhydrides such as ReH_7 , $Re(OH)H_6$, ReH_5 , and ReH_6 are found to be of lower energy toward higher $\Delta\mu_H$ values (-0.5 to -0.2 eV). Among these, ReH_7 is found to be the most feasible species ([Figure 4a](#)). In a $\Delta\mu_H$ range of -0.72 to -0.65 eV, $Re(OH)H_6$ is found to be the prominent species. In the intermediate range of -0.65 to -0.5 eV, a mixture of ReH_7 and $Re(OH)H_6$ coexists.

Re species with specific oxidation states ranging from 0 to +7 were individually analyzed further. Under oxidizing conditions (at low $\Delta\mu_H$), the formation of oxygenated species is energetically preferred across all oxidation states, following a trend similar to that observed above. Despite the oxophilic nature of Re, these oxygenated species are highly destabilized in a H_2 -rich environment, making hydrides the most stable species. Even under highly reducing conditions, Re species with lower formal oxidation states are highly unfavorable. For instance, all species with Re oxidation states from 0 to +4 are destabilized by more than 1 eV compared to the stable hydride species at 1 bar of H_2 and 400 K. Note that an elevated pressure of 1 bar for water is employed in these analyses to assess whether highly oxidizing conditions would have any significant impact. However, even under these extreme oxidizing conditions, the energetic trends remained consistent with those observed under a highly reducing H_2 atmosphere.

As shown in [eq 1](#), water is formed as a side product during reduction of the Re_2O_7 precatalyst. Hence, the stability of active species is also analyzed with respect to the change in the chemical potential of water ($\Delta\mu_{H_2O}$). Under reducing conditions, more oxygen ligands on the precatalytic Re could be removed as water, leading to the formation of polyhydrides. In line with this assumption, ReH_7 , ReH_6 , and ReH_5 are identified as lower-energy species at low $\Delta\mu_{H_2O}$ values (below -1.6 eV). However, as the system becomes more water-rich, $Re(OH)H_6$ ($\Delta\mu_{H_2O}$ range of -1.5 to -1.1 eV) and subsequently ReO_3 ($\Delta\mu_{H_2O}$ higher than -1.1 eV) become the most stable species. See [Figure S3](#) in the [Supporting Information](#). This trend is attributed to the oxophilic nature of Re. In a water-rich environment, Re–H bonds in polyhydrides may undergo sigma-bond metathesis with water molecules to form Re–OH bonds, which could eventually transform to form Re–O. Therefore, an equilibrium might form in the reaction system between Re polyhydrides, hydroxo-ligated polyhydrides, and oxide in humid conditions.

The results of the aiTD analysis are in line with experimental studies proposing the existence of multiple oxidation states of Re in the active species. In summary, a H_2 -rich environment

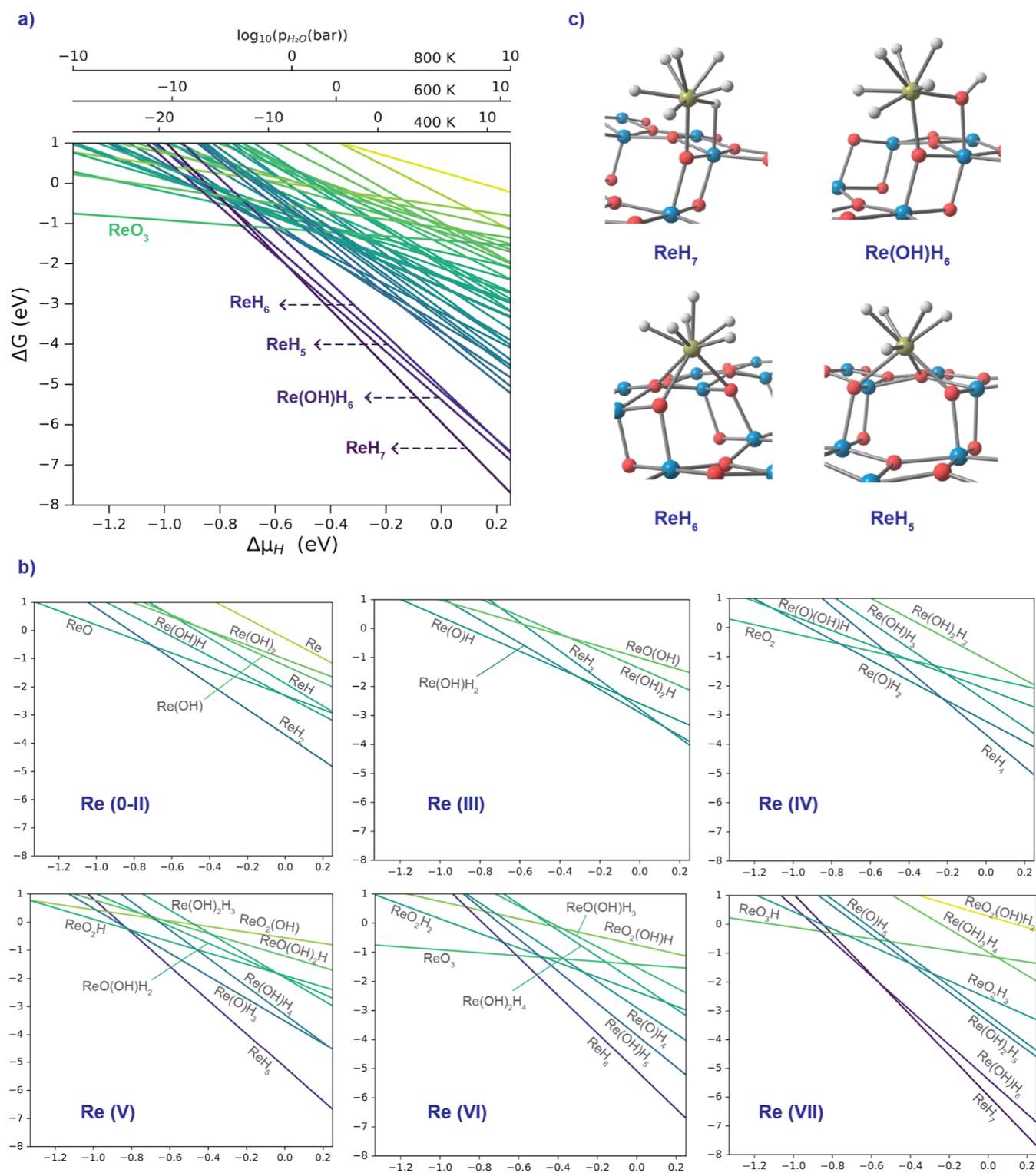


Figure 4. (a) Gibbs free energy profile for Re active species across oxidation states (0 to +7) as a function of hydrogen chemical potential ($\Delta\mu_H$) at a fixed water chemical potential ($\Delta\mu_{\text{H}_2\text{O}}$) corresponding to 1 bar H_2O at 800 K on the $\text{TiO}_2\text{-d}$ surface. (b) Specific Gibbs free energy profiles for distinct Re oxidation states. (c) DFT-optimized geometries of the most stable surface-bound Re species, as determined from the aiTD analysis.

promotes the hydrogenation and hydrogenolysis of the Re precatalyst, leading to the replacement of oxygen ligands with hydroxides or hydrides while maintaining the high formal oxidation state of Re. Surprisingly, in contrast to the XPS characterizations, we do not observe Re in low formal oxidation states. Hence, we decided to analyze the effect of

varying the chemical environment, specifically the change in ligands, on the electronic structure of the Re species.

3.3. Charge Analysis. Bader charges⁵² of a few representative Re active species adsorbed on the $\text{TiO}_2\text{-d}$ surface were analyzed and compared with bulk Re reference species with a well-defined structure and established oxidation

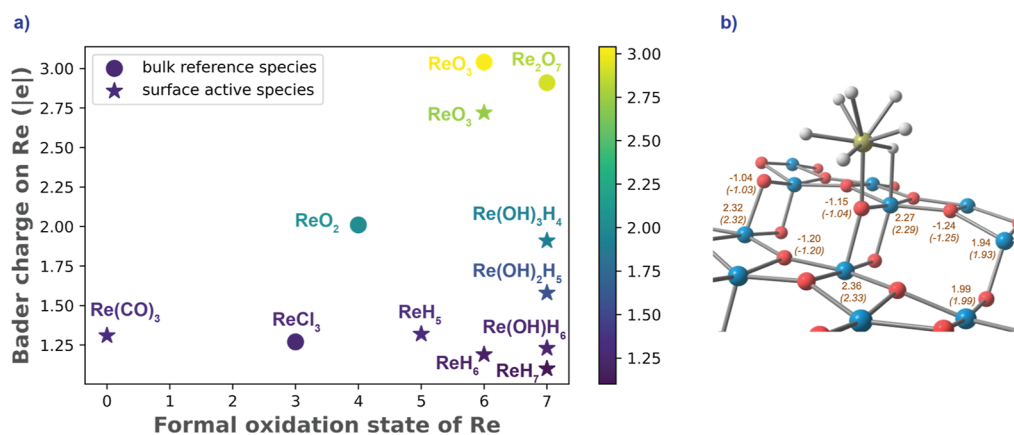


Figure 5. (a) Calculated Bader charges for different surface and bulk Re species; (b) comparison of Bader charges on TiO_2 -d surface atoms before and after the active species ReH_7 formation. Bader charge without active species is shown in parentheses.

state such as ReCl_3 , ReO_2 , ReO_3 , and Re_2O_7 .⁵³ It is observed that the Re center becomes electron-rich as the number of hydride ligands increases on the adsorbed species, as shown in Figure 5a. The Re center in surface species ReH_5 has a higher positive charge than ReH_6 , which in turn is more positively charged than ReH_7 . This trend is consistent with alternative charge partitioning using the density derived electrostatic and chemical (DDEC6) charges^{54–56} method, as shown in Table S3 in the Supporting Information.

A comparison of Bader charges on the surface atoms of bare TiO_2 -d and those with adsorbed surface species was conducted to determine if charge transfer from the surface results in an electron-rich Re center. However, the surface O atom where the Re species is adsorbed became less positive than the bare surface. The surrounding O and Ti atoms show no significant change in charge, as demonstrated for ReH_7 in Figure 5b. This suggests that the strong donor hydride ligands effectively enhance the electron density on Re, even though it is in a highly formal oxidation state.

The extent of charge transfer in polyhydrides can be envisaged by the comparable charge on Re in adsorbed $\text{Re}(\text{CO})_3$ which has a formal oxidation state of 0. Interestingly, charges on Re in ReH_7 , ReH_6 , ReH_5 , $\text{Re}(\text{OH})\text{H}_6$, and $\text{Re}(\text{CO})_3$ are 1.10, 1.19, 1.32, 1.23, and 1.31, respectively, comparable to that of bulk ReCl_3 (1.27) whose formal oxidation state is +3. The Re charge on adsorbed ReO_3 (2.72), devoid of any electron-donating hydride ligand, is comparable to that of bulk ReO_3 (3.04). Although the stable polyhydrides have a high formal oxidation state ranging from +5 to +7, their electronic nature varies significantly from the corresponding bulk structure, as indicated by the charge analysis. Moreover, the most stable polyhydride ReH_7 species features comparable charge on Re to that in $\text{Re}(\text{CO})_3$, a surface intermediate proposed in prior experimental studies.¹⁰ This intriguing observation prompted us to investigate the potential XPS signatures of these diverse species.

3.4. XPS Calculation. XPS analysis has been widely employed to analyze the electronic nature of Re on a surface.^{17,57} Hence, XPS simulations were performed to calculate the Re 4f binding energy for various rhenium species. From the calculations, the binding energy for $\text{Re}(\text{CO})_3$, where rhenium has a formal oxidation state of zero, is found to be 44.1 eV (Table 1). The feasible surface species ReH_7 and $\text{Re}(\text{OH})\text{H}_6$ in formal +7 state exhibit a binding energy of 43.0 and 43.6 eV. ReH_5 in the +5 state and ReO_3 in the +6 state

Table 1. Calculated Re 4f Binding Energy for Different Re Species

active species on TiO_2 -d	Re formal oxidation state	Bader charge on Re	Re 4f binding energy (eV)
$\text{Re}(\text{CO})_3$	0	1.31	44.1
ReH_5	+5	1.32	42.4
ReO_3	+6	2.72	46.1
ReH_7	+7	1.10	43.0
$\text{Re}(\text{OH})\text{H}_6$	+7	1.23	43.6
$\text{Re}(\text{OH})_2\text{H}_5$	+7	1.58	44.3
$\text{Re}(\text{OH})_3\text{H}_4$	+7	1.91	44.1

have a binding energy of 42.4 and 46.1 eV, respectively. The analysis was expanded to include two higher-energy species with a formal +7 oxidation state: $\text{Re}(\text{OH})_2\text{H}_5$ and $\text{Re}(\text{OH})_3\text{H}_4$. Interestingly, the calculated binding energy for $\text{Re}(\text{OH})_3\text{H}_4$ (44.1 eV) is equal to that of $\text{Re}(\text{CO})_3$. The binding energy for $\text{Re}(\text{OH})_2\text{H}_5$ is only 0.2 eV higher than that of $\text{Re}(\text{CO})_3$.

The experimentally measured binding energies for $\text{Re}(0)$ in the range of 40–41 eV are lower than the calculated value for $\text{Re}(\text{CO})_3$.^{10,17,22,24,58,59} The formation of metal nanoparticles and clusters on the surface could lead to lower-energy values, but these species are outside the scope of this study and, thus, not considered. The calculated value for highly oxidized ReO_3 aligns well with the experimentally observed range of 43.1–45.5 eV. Interestingly, the computed binding energies for the polyhydrides are lower than the experimental values for Re species in a similar formal oxidation state. For instance, ReH_7 is 2.5–3.5 eV below the experimentally determined range of 45.5–46.5 eV for $\text{Re}(+7)$.^{10,17,22–25,59,60} Notably, the calculated binding energy for ReH_7 in the formal oxidation state of +7 is lower than that of ReO_3 in the +6 state. This suggests that the XPS signals of reduced polyhydride species shift to a lower-energy region where lower formal oxidation states are typically observed experimentally.

The computed values indicate that the binding energy is more related to the charge on Re (Figure 6) than the formal oxidation state (Table 1). Re with a higher positive charge leads to a higher binding energy except for ReH_5 . ReH_5 has a higher positive charge than ReH_7 but shows a lower binding energy than ReH_7 . The overall trend is consistent with general XPS trends that as ligands with higher electronegativity (such as O) draw metal valence electrons strongly away from metal

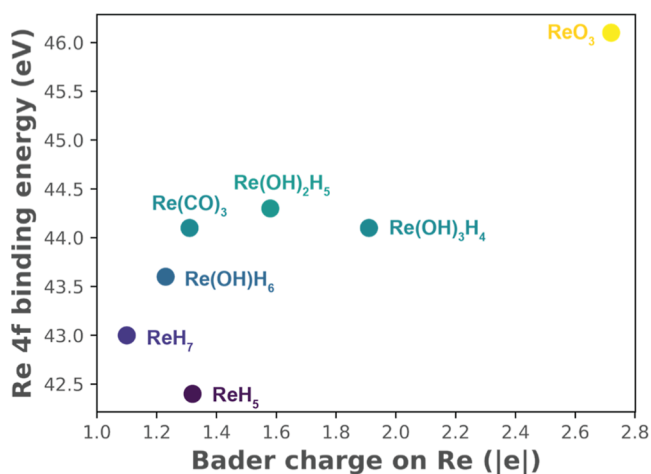


Figure 6. Change in Re 4f binding energy with Bader charge for different surface Re species.

center, effective nuclear charge increases, and thus, it increases binding energy. This implies that the spectroscopic signature obtained from XPS analysis is highly dependent on the ligand environment, leading to the observation that Re with different formal oxidation states can show similar spectroscopic signatures depending on the ligands present. Consequently, the spectroscopic analysis of these surface species can be complex and challenging due to the significant influence of the ligand environment on the binding energies.

3.5. Reactivity. Reactivity of the stable active species toward CO₂ reduction was explored further with a representative ReH₇ species. The investigated reaction steps include CO₂ adsorption on the surface, reduction of CO₂ through hydride or proton transfer, and the subsequent formation of formate or carboxyl intermediates on the TiO₂ surface. CO₂ can adsorb onto the TiO₂ support in two

configurations: a linear arrangement, where one of the oxygens interacts with a single Ti center on the surface, or a bent arrangement, where both oxygen and the carbon atom of CO₂ interact with surface Ti centers (Figure 7). In the linear arrangement, the adsorption energy on the TiO₂-p and TiO₂-d surface is -46 and -57 kJ/mol, respectively. On the TiO₂-d surface, adsorption of CO₂ on a Ti center with an oxygen vacancy defect is considered. The activation barriers for hydride insertion into CO₂ for ReH₇ on TiO₂-p and TiO₂-d are 39 and 32 kJ/mol. Such low reaction barriers demonstrate the high reactivity of the surface species in facilitating hydride insertion into CO₂. The evaluation of reaction energy reveals that the formation of the formate intermediate is an exothermic process. Other stable surface-active species also exhibit similar reactivity toward CO₂ activation, as shown in Table S4 and Figure S5 in the Supporting Information.

CO₂ to form a carboxyl intermediate was also analyzed. CO₂ adsorption in a bent configuration partially activates CO₂ by geometrical distortion where the C=O is elongated in the adsorbed species (Figure 7b). This adsorption geometry is strongly favored thermodynamically for the defected TiO₂ support, while for the *p*-TiO₂, the linear adsorption is preferred. The strongly coordinated CO₂ in the bent geometry can be further transformed to the carboxyl intermediate via a formal proton transfer from ReH₇. The activation energy associated with this process is 147 and 154 kJ/mol, respectively, on TiO₂-p and TiO₂-d, higher than 100 kJ/mol to that of the formate path. The carboxyl pathway is endothermic as shown in Figure 7a, indicating that this higher barrier pathway could coexist with the formate pathway at a higher temperature according to Le-Chatelier's principle. In summary, the lowest-energy surface species identified from the aiTD analysis are capable of activating CO₂ as indicated by the energy barriers calculated for the formate and carboxyl pathways.

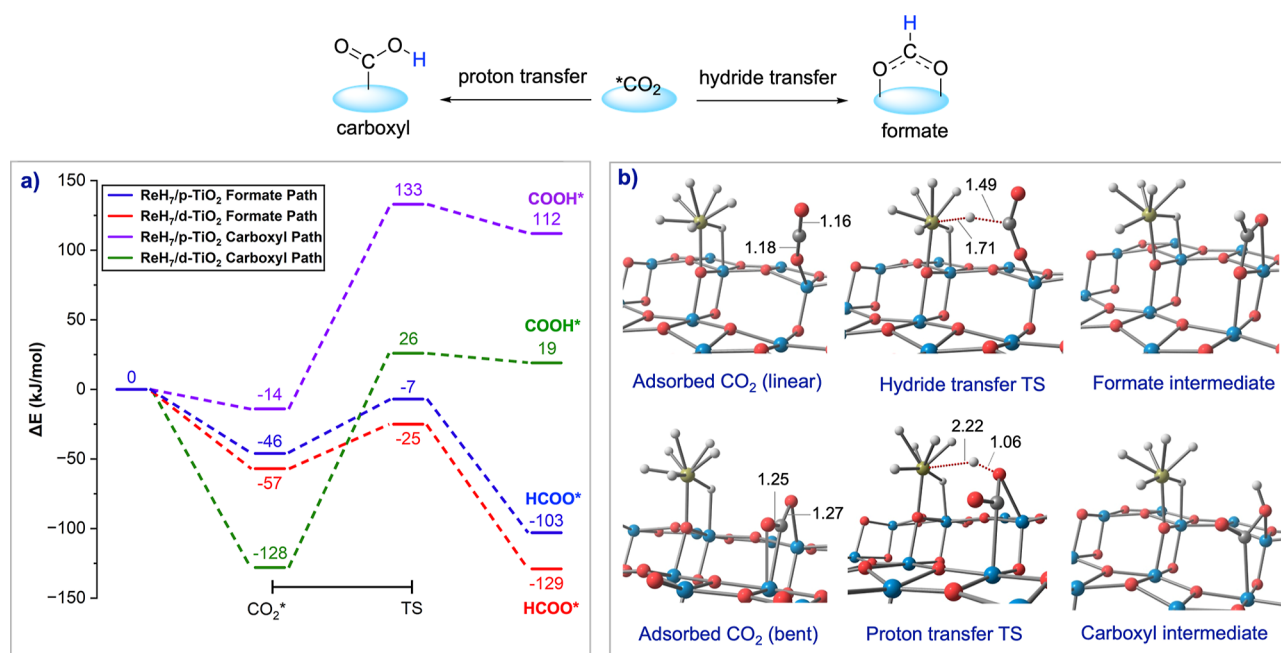


Figure 7. (a) Computed reaction energy (kJ/mol) profile for the activation of CO₂ to formate and carboxyl intermediates by ReH₇ on TiO₂-p and TiO₂-d, and (b) DFT-optimized geometries of key intermediates and transition states involved in the activation of CO₂, leading to the formation of formate and carboxyl intermediates.

4. CONCLUSIONS

This study explores the various possible single-site Re active species formed by the hydrogenation of Re_2O_7 on the TiO_2 surface. Through aiTD analysis, polyhydride species such as ReH_7 , $\text{Re}(\text{OH})\text{H}_6$, ReH_5 , and ReH_6 are identified as the stable species formed on the surface. This indicates that the oxygen ligands on the Re precursor are effectively exchanging with the hydrides under a hydrogen-rich atmosphere. Even under the highly reducing hydrogen atmosphere conditions, Re species with low formal oxidation states are found to be highly unstable. The aiTD results deducing multiple stable Re species in high formal oxidation states (+5 to +7) on the support are in line with many experimental observations. All stable surface rhenium polyhydride species identified through aiTD analysis are providing facile routes for activating CO_2 as formate via hydrogenation with low activation barriers. In the presence of oxygen vacancies near the single-site Re species on defect TiO_2 , CO_2 preferentially adsorbs to reduced Ti sites in a bent geometry that opens alternative activation carboxyl paths.

The electronic properties of the surface-active species are found to be strongly dependent on the ligand environment. The presence of hydride ligands renders the Re metal center electron-rich. Specifically, the Bader charge on the formally +7 Re species in stable ReH_7 is even lower than that on the formally metallic Re in $\text{Re}(\text{CO})_3$ species. These trends in the atomic charges are also reflected by the computed XPS signatures, highlighting the limited applicability and utility of the formal oxidation state formalism for the description of such surface species. The comparable stability of multiple Re complexes featuring different coordination states and varied ligand environments makes the assignment of “single-site” simplified characteristics to the observed Re surface species very challenging. In particular, our results demonstrate the limitations of routine interpretation of the experimental XPS characterization data of such heterogeneous catalyst materials, in terms of formal oxidation states and oversimplified chemical models.

■ ASSOCIATED CONTENT

Data Availability Statement

Data related to this work is openly available via the 4TU repository under the DOI: [10.4121/198a447c-78a0-4728-b05e-d2a89beaf1ff](https://doi.org/10.4121/198a447c-78a0-4728-b05e-d2a89beaf1ff).

SI Supporting Information

The Supporting Information is available free of charge at <https://pubs.acs.org/doi/10.1021/acscatal.4c05697>.

Optimized structures in the VASP POSCAR format (ZIP)

Compilation of reaction schemes, formation energies, aiTD analysis, and energetics associated with CO_2 activation for different active species (PDF)

■ AUTHOR INFORMATION

Corresponding Authors

A. Sreenithya – *Inorganic Systems Engineering, Department of Chemical Engineering, Faculty of Applied Sciences, Delft University of Technology, Delft 2629 HZ, Netherlands;* orcid.org/0000-0001-8598-291X; Email: s.avadakkam@tudelft.nl

Evgeny A. Pidko – *Inorganic Systems Engineering, Department of Chemical Engineering, Faculty of Applied Sciences, Delft University of Technology, Delft 2629 HZ,*

Netherlands; orcid.org/0000-0001-9242-9901;

Email: e.a.pidko@tudelft.nl

Authors

Alexander A. Kolganov – *Inorganic Systems Engineering, Department of Chemical Engineering, Faculty of Applied Sciences, Delft University of Technology, Delft 2629 HZ, Netherlands;* orcid.org/0000-0002-0262-8892

In Won Yeu – *Department of Chemical Engineering, Columbia University, New York, New York 10027, United States*

Muhammad Helmi Risansyaqi – *Inorganic Systems Engineering, Department of Chemical Engineering, Faculty of Applied Sciences, Delft University of Technology, Delft 2629 HZ, Netherlands*

Complete contact information is available at:

<https://pubs.acs.org/10.1021/acscatal.4c05697>

Author Contributions

The manuscript was written through contributions of all authors. All authors have given approval to the final version of the manuscript.

Notes

The authors declare no competing financial interest.

■ ACKNOWLEDGMENTS

A.S. thanks Dr. Jittima Meeprasert for the discussions and technical inputs at the start of this project. The authors thank Prof. Alexander Urban, Department of Chemical Engineering, Columbia University, for the valuable discussions and inputs. The authors thank Advanced Research Center Chemical Building Blocks Consortium (ARC CBBC) for supporting this research under project number 2021.038.C.

■ REFERENCES

- (1) Gothe, M. L.; Silva, K. L. C.; Figueredo, A. L.; Fiorio, J. L.; Rozendo, J.; Manduca, B.; Simizu, V.; Freire, R. S.; Garcia, M. A. S.; Vidinha, P. Rhenium – A Tuneable Player in Tailored Hydrogenation Catalysis. *Eur. J. Inorg. Chem.* **2021**, *2021*, 4043–4065.
- (2) Luo, J.; Liang, C. Rhenium in Heterogeneous Catalysis: A Rising Star for Hydrogenation Reactions. *ACS Catal.* **2024**, *14*, 7032–7049.
- (3) Tomishige, K.; Nakagawa, Y.; Tamura, M. Taming Heterogeneous Rhenium Catalysis for the Production of Biomass-Derived Chemicals. *Chin. Chem. Lett.* **2020**, *31*, 1071–1077.
- (4) Ojeda, J.; Escalona, N.; Fierro, J. L. G.; Agudo, A. L.; Gil-Lambias, F. J. Effect of the Preparation of $\text{Re}/\gamma\text{-Al}_2\text{O}_3$ Catalysts on the HDS and HDN of Gas Oil. *Appl. Catal., A* **2005**, *281*, 25–30.
- (5) Sepulveda, C.; Bellière, V.; Laurenti, D.; Escalona, N.; García, R.; Geantet, C.; Vrinat, M. Supported Rhenium Sulfide Catalysts in Thiophene and 4,6-Dimethyldibenzothiophene Hydrodesulfurization: Effect of Acidity of the Support over Activities. *Appl. Catal., A* **2011**, *393*, 288–293.
- (6) Sureshkumar, K.; Shanthi, K.; Sasirekha, N. R.; Jegan, J.; Sardhar Basha, S. J. A Study on Catalytic Activity of Modified Ni–Re/Al-SBA-15 Catalyst for Hydrodenitrogenation of o-Toluidine. *Int. J. Hydrogen Energy* **2020**, *45*, 4328–4340.
- (7) Jia, X.; Qin, C.; Friedberger, T.; Guan, Z.; Huang, Z. Efficient and Selective Degradation of Polyethylenes into Liquid Fuels and Waxes under Mild Conditions. *Sci. Adv.* **2016**, *2*, No. e1501591.
- (8) Mol, J. C. Olefin Metathesis over Supported Rhenium Oxide Catalysts. *Catal. Today* **1999**, *51*, 289–299.
- (9) Ting, K. W.; Toyao, T.; Siddiki, S. M. A. H.; Shimizu, K. I. Low-Temperature Hydrogenation of CO_2 to Methanol over Heterogeneous TiO_2 -Supported Re Catalysts. *ACS Catal.* **2019**, *9*, 3685–3693.

- (10) Phongprueksathat, N.; Ting, K. W.; Mine, S.; Jing, Y.; Toyoshima, R.; Kondoh, H.; Shimizu, K. I.; Toyao, T.; Urakawa, A. Bifunctionality of Re Supported on TiO₂ in Driving Methanol Formation in Low-Temperature CO₂ Hydrogenation. *ACS Catal.* **2023**, *13*, 10734–10750.
- (11) Bare, S. R.; Kelly, S. D.; D.vila, F.; Boldingh, E.; Karapetrova, E.; Kas, J.; Mickelson, G. E.; Modica, F. S.; Yang, N.; Rehr, J. J. Experimental (XAS, STEM, TPR, and XPS) and Theoretical (DFT) Characterization of Supported Rhenium Catalysts. *J. Phys. Chem. C* **2011**, *115*, 5740–5755.
- (12) Copéret, C.; Berkson, Z. J.; Chan, K. W.; de Jesus Silva, J.; Gordon, C. P.; Pucino, M.; Zhizhko, P. A.; Pucino, M.; Zhizhko, P. A. Olefin Metathesis: What Have We Learned about Homogeneous and Heterogeneous Catalysts from Surface Organometallic Chemistry? *Chem. Sci.* **2021**, *12*, 3092–3115.
- (13) Lwin, S.; Keturakis, C.; Handzlik, J.; Sautet, P.; Li, Y.; Frenkel, A. I.; Wachs, I. E. Surface ReOx Sites on Al₂O₃ and Their Molecular Structure-Reactivity Relationships for Olefin Metathesis. *ACS Catal.* **2015**, *5*, 1432–1444.
- (14) Zhang, B.; Wachs, I. E. Identifying the Catalytic Active Site for Propylene Metathesis by Supported ReOx catalysts. *ACS Catal.* **2021**, *11*, 1962–1976.
- (15) Shen, C.; Sun, K.; Zou, R.; Wu, Q.; Mei, D.; Liu, C. J. CO₂ Hydrogenation to Methanol on Indium Oxide-Supported Rhenium Catalysts: The Effects of Size. *ACS Catal.* **2022**, *12*, 12658–12669.
- (16) Liu, B.; Sekine, N.; Nakagawa, Y.; Tamura, M.; Yabushita, M.; Tomishige, K. Synthesis of Secondary Monoalcohols from Terminal Vicinal Alcohols over Silica-Supported Rhenium-Modified Ruthenium Catalyst. *ACS Sustain. Chem. Eng.* **2022**, *10*, 1220–1231.
- (17) Liu, K.; Pritchard, J.; Lu, L.; Van Putten, R.; Tiny Verhoeven, M. W. G. M.; Schmitkamp, M.; Huang, X.; Lefort, L.; Kiely, C. J.; Hensen, E. J. M.; Pidko, E. A. Supported Nickel–Rhenium Catalysts for Selective Hydrogenation of Methyl Esters to Alcohols. *Chem. Commun.* **2017**, *53*, 9761–9764.
- (18) Pritchard, J.; Ciftci, A.; Verhoeven, M. W. G. M. T.; Hensen, E. J. M.; Pidko, E. A. Supported Pt-Re Catalysts for the Selective Hydrogenation of Methyl and Ethyl Esters to Alcohols. *Catal. Today* **2017**, *279*, 10–18.
- (19) Okal, J.; Tylus, W.; Kępiński, L. XPS Study of Oxidation of Rhenium Metal on γ -Al₂O₃ Support. *J. Catal.* **2004**, *225*, 498–509.
- (20) Veerakumar, P.; Thanasekaran, P.; Lin, K. C.; Liu, S. B. Well-Dispersed Rhenium Nanoparticles on Three-Dimensional Carbon Nanostructures: Efficient Catalysts for the Reduction of Aromatic Nitro Compounds. *J. Colloid Interface Sci.* **2017**, *506*, 271–282.
- (21) Rimoldi, M.; Hupp, J. T.; Farha, O. K. Atomic Layer Deposition of Rhenium-Aluminum Oxide Thin Films and ReOx Incorporation in a Metal-Organic Framework. *ACS Appl. Mater. Interfaces* **2017**, *9*, 35067–35074.
- (22) Toyao, T.; Siddiki, S. M. A. H.; Morita, Y.; Kamachi, T.; Touchy, A. S.; Onodera, W.; Kon, K.; Furukawa, S.; Ariga, H.; Asakura, K.; Yoshizawa, K.; Shimizu, K. I. Rhenium-Loaded TiO₂: A Highly Versatile and Chemoselective Catalyst for the Hydrogenation of Carboxylic Acid Derivatives and the N-Methylation of Amines Using H₂ and CO₂. *Chem.—Eur. J.* **2017**, *23*, 14848–14859.
- (23) Ota, N.; Tamura, M.; Nakagawa, Y.; Okumura, K.; Tomishige, K. Performance, Structure, and Mechanism of ReOx-Pd/CeO₂ Catalyst for Simultaneous Removal of Vicinal OH Groups with H₂. *ACS Catal.* **2016**, *6*, 3213–3226.
- (24) Huang, X.; Liu, K.; Vrijburg, W. L.; Ouyang, X.; Iulian Dugulan, A.; Liu, Y.; Tiny Verhoeven, M. W. G. M.; Kosinov, N. A.; Pidko, E. A.; Hensen, E. J. M. Hydrogenation of Levulinic Acid to γ -Valerolactone over Fe-Re/TiO₂ Catalysts. *Appl. Catal., B* **2020**, *278*, 119314.
- (25) Gothe, M. L.; Pérez-Sanz, F. J.; Braga, A. H.; Borges, L. R.; Abreu, T. F.; Bazito, R. C.; Gonçalves, R. V.; Rossi, L. M.; Vidinha, P. Selective CO₂ Hydrogenation into Methanol in a Supercritical Flow Process. *J. CO₂ Util.* **2020**, *40*, 101195.
- (26) Kresse, G.; Joubert, D. From Ultrasoft Pseudopotentials to the Projector Augmented-Wave Method. *Phys. Rev. B:Condens. Matter Mater. Phys.* **1999**, *59*, 1758.
- (27) Kresse, G.; Furthmüller, J. Efficient Iterative Schemes for Ab Initio Total-Energy Calculations Using a Plane-Wave Basis Set. *Phys. Rev. B:Condens. Matter Mater. Phys.* **1996**, *54*, 11169.
- (28) Ataei, S. S.; Mohammadzadeh, M. R.; Seriani, N. Ab Initio Simulation of the Effects of Hydrogen Concentration on Anatase TiO₂. *J. Phys. Chem. C* **2016**, *120*, 8421–8427.
- (29) Bourikas, K.; Kordulis, C.; Lycourghiotis, A. Titanium Dioxide (Anatase and Rutile): Surface Chemistry, Liquid-Solid Interface Chemistry, and Scientific Synthesis of Supported Catalysts. *Chem. Rev.* **2014**, *114*, 9754–9823.
- (30) Diebold, U. The Surface Science of Titanium Dioxide. *Surf. Sci. Rep.* **2003**, *48*, 53–229.
- (31) Sorescu, D. C.; Al-Saidi, W. A.; Jordan, K. D. CO₂ Adsorption on TiO₂(101) Anatase: A Dispersion-Corrected Density Functional Theory Study. *J. Chem. Phys.* **2011**, *135*, 124701.
- (32) Esch, T. R.; Gadaczek, I.; Bredow, T. Surface Structures and Thermodynamics of Low-Index of Rutile, Brookite and Anatase – A Comparative DFT Study. *Appl. Surf. Sci.* **2014**, *288*, 275–287.
- (33) Aschauer, U.; Selloni, A. Hydrogen Interaction with the Anatase TiO₂(101) Surface. *Phys. Chem. Chem. Phys.* **2012**, *14*, 16595–16602.
- (34) Ip, C. M.; Troisi, A. A. Computational Study of the Competing Reaction Mechanisms of the Photo-Catalytic Reduction of CO₂ on Anatase(101). *Phys. Chem. Chem. Phys.* **2016**, *18*, 25010–25021.
- (35) Li, Q.; Yan, G.; Vlachos, D. G. Theoretical Insights into H₂ Activation over Anatase TiO₂ Supported Metal Adatoms. *ACS Catal.* **2024**, *14*, 886–896.
- (36) Geng, Z.; Chen, X.; Yang, W.; Guo, Q.; Xu, C.; Dai, D.; Yang, X. Highly Efficient Water Dissociation on Anatase TiO₂(101). *J. Phys. Chem. C* **2016**, *120*, 26807–26813.
- (37) Li, G.; Meeprasert, J.; Wang, J.; Li, C.; Pidko, E. A. CO₂ Hydrogenation to Methanol over Cd₄/TiO₂ Catalyst: Insight into Multifunctional Interface. *ChemCatChem* **2022**, *14*, No. e202101646.
- (38) NIST-JANAF Thermochemical Tables. <https://janaf.nist.gov/> (accessed July 26, 2024).
- (39) Reuter, K.; Scheffler, M. Composition, Structure, and Stability of RuO₂ (110) as a Function of Oxygen Pressure. *Phys. Rev. B:Condens. Matter Mater. Phys.* **2001**, *65*, 035406.
- (40) Reuter, K. Ab Initio Thermodynamics and First-Principles Microkinetics for Surface Catalysis. *Catal. Lett.* **2016**, *146*, 541–563.
- (41) Li, H.; Reuter, K. Ab Initio Thermodynamic Stability of Carbide Catalysts under Electrochemical Conditions. *ACS Catal.* **2022**, *12*, 10506–10513.
- (42) Grajciar, L.; Heard, C. J.; Bondarenko, A. A.; Polynski, M. V.; Meeprasert, J.; Pidko, E. A.; Nachtigall, P. Towards Operando Computational Modeling in Heterogeneous Catalysis. *Chem. Soc. Rev.* **2018**, *47*, 8307–8348.
- (43) Blum, V.; Gehrke, R.; Hanke, F.; Havu, P.; Havu, V.; Ren, X.; Reuter, K.; Scheffler, M. Ab Initio Molecular Simulations with Numeric Atom-Centered Orbitals. *Comput. Phys. Commun.* **2009**, *180*, 2175–2196.
- (44) Havu, V.; Blum, V.; Havu, P.; Scheffler, M. Efficient O(N) Integration for All-Electron Electronic Structure Calculation Using Numeric Basis Functions. *J. Comput. Phys.* **2009**, *228*, 8367–8379.
- (45) Strange, R.; Manby, F. R.; Knowles, P. J. Automatic Code Generation in Density Functional Theory. *Comput. Phys. Commun.* **2001**, *136*, 310–318.
- (46) Golze, D.; Keller, L.; Rinke, P. Accurate Absolute and Relative Core-Level Binding Energies from GW. *J. Phys. Chem. Lett.* **2020**, *11*, 1840–1847.
- (47) Van Lenthe, E.; Baerends, E. J.; Snijders, J. G. Relativistic Total Energy Using Regular Approximations. *J. Chem. Phys.* **1994**, *101*, 9783–9792.
- (48) Harrath, K.; Yu, X.; Xiao, H.; Li, J. The Key Role of Support Surface Hydrogenation in the CH₄ to CH₃OH Selective Oxidation by

a ZrO₂-Supported Single-Atom Catalyst. *ACS Catal.* **2019**, *9*, 8903–8909.

(49) Polo-Garzon, F.; Bao, Z.; Zhang, X.; Huang, W.; Wu, Z. Surface Reconstructions of Metal Oxides and the Consequences on Catalytic Chemistry. *ACS Catal.* **2019**, *9*, 5692–5707.

(50) Wu, L.; Fu, C.; Huang, W. Surface Chemistry of TiO₂ Connecting Thermal Catalysis and Photocatalysis. *Phys. Chem. Chem. Phys.* **2020**, *22*, 9875–9909.

(51) Islam, M. M.; Calatayud, M.; Pacchioni, G. Hydrogen Adsorption and Diffusion on the Anatase TiO₂(101) Surface: A First-Principles Investigation. *J. Phys. Chem. C* **2011**, *115*, 6809–6814.

(52) Bader, R. F. W. *Atoms in Molecules: A Quantum Theory*; Oxford University Press, 1990; p 438.

(53) Ting, K. W.; Mine, S.; Ait El Fakir, A.; Du, P.; Li, L.; Siddiki, S. M. A. H.; Toyao, T.; Shimizu, K. The Reducibility and Oxidation States of Oxide-Supported Rhenium: Experimental and Theoretical Investigations. *Phys. Chem. Chem. Phys.* **2022**, *24*, 28621–28631.

(54) Manz, T. A.; Sholl, D. S. Improved Atoms-in-Molecule Charge Partitioning Functional for Simultaneously Reproducing the Electrostatic Potential and Chemical States in Periodic and Nonperiodic Materials. *J. Chem. Theory Comput.* **2012**, *8*, 2844–2867.

(55) Chen, D. L.; Stern, A. C.; Space, B.; Johnson, J. K. Atomic Charges Derived from Electrostatic Potentials for Molecular and Periodic Systems. *J. Phys. Chem. A* **2010**, *114*, 10225–10233.

(56) Wang, B.; Li, S. L.; Truhlar, D. G. Modeling the Partial Atomic Charges in Inorganometallic Molecules and Solids and Charge Redistribution in Lithium-Ion Cathodes. *J. Chem. Theory Comput.* **2014**, *10*, 5640–5650.

(57) Yuan, Y.; Shido, T.; Iwasawa, Y. The New Catalytic Property of Supported Rhenium Oxides for Selective Oxidation of Methanol to Methylal. *Chem. Commun.* **2000**, 1421–1422.

(58) Suknev, A.; Zaikovskii, V.; Kaichev, V.; Paukshtis, E.; Sadovszkaya, E.; Bal'Zhinimaev, B. The Nature of Active Sites in Pt–ReO_x/TiO₂ Catalysts for Selective Hydrogenation of Carboxylic Acids to Alcohols. *J. Energy Chem.* **2015**, *24*, 646–654.

(59) Greiner, M. T.; Rocha, T. C. R.; Johnson, B.; Klyushin, A.; Knop-Gericke, A.; Schlögl, R. The Oxidation of Rhenium and Identification of Rhenium Oxides during Catalytic Partial Oxidation of Ethylene: An in-Situ XPS Study. *Z. Phys. Chem.* **2014**, *228*, 521–541.

(60) Avramescu, S.; Ene, C. D.; Ciobanu, M.; Schnee, J.; Devred, F.; Bucur, C.; Vasile, E.; Colaciello, L.; Richards, R.; Gaigneaux, E. M.; Verziu, M. N. Nanocrystalline Rhenium-Doped TiO₂: An Efficient Catalyst in the One-Pot Conversion of Carbohydrates into Levulinic Acid. The Synergistic Effect between Brønsted and Lewis Acid Sites. *Catal. Sci. Technol.* **2022**, *12*, 167–180.